ELSEVIER

S0032-3861(96)00316-3

Polymer Vol. 37 No. 21, pp. 4823–4831, 1996

0032-3861/96/$15.00 + 0.00

Microporous polymeric materials by microemulsion polymerization: effect of the ratio of long and short alkyl chain length cationic surfactants

T. H. Chieng*, L. M. Gan, C. H. Chew, S. C. Ng† and K. L. Pey‡
Department of Chemistry, †Department of Physics, ‡Institute of Microelectronics, National University of Singapore, 10 Kent Ridge Road, Singapore 119260, Republic of Singapore
(Received 20 December 1995; revised 6 January 1996)

Bicontinuous microemulsions consisting of methyl methacrylate, 2-hydroxyethyl methacrylate, ethylene glycol dimethacrylate, and water mixtures of long and short alkyl chain length cationic *n*-alkyltrimethylammonium bromides as surface-active agent, were used as precursors for the formation of porous polymeric materials. It was found that the mixing ratio of long and short chain length surfactants has a pronounced influence on the morphology and microstructure of the polymeric materials so obtained. At a particular ratio of long to short alkyl chain length cationic surfactants, the pores were found to be irregular and sponge-like in structure resembling that of a bicontinuous structure. All electron microscopy investigation, swelling and permeability studies indicate an increase in pore sizes of the polymeric materials on increasing the weight ratio of long chain length relative to that of short chain length surfactant. The modification in the microstructure of the polymeric materials is discussed in terms of the interfacial film rigidity. Copyright © 1996 Elsevier Science Ltd.

(Keywords: bicontinuous microemulsions; morphology and microstructure; polymeric materials)

INTRODUCTION

Since the introduction by Scriven[1], there has been much evidence indicating the existence of bicontinuous microemulsions. A direct proof was given by Jahn *et al.*[2] who studied nonionic microemulsions. Their electron photomicrographs clearly show the bicontinuity between the aqueous and oily domains. Indirect evidence was given by viscosity, n.m.r. and self-diffusion experiments[3,4]. The bicontinuous structure is commonly described as an irregular sponge-like structure in which aqueous and oily domains are interconnected over macroscopic distances or are locally lamellar[1,5]. Various models have been proposed to account for the formation and behaviour of the structure[6,7]. It is noteworthy that the interfacial film of a bicontinuous structure has a zero mean curvature, i.e. it is flat on average[8].

Apart from extensive studies on bicontinuous microemulsions themselves, they have been employed to prepare transparent, stable and fluid microlatexes when the amount of monomer(s) reached 25% and that of surfactant is reduced to about 10%[9,10]. A bicontinuous microemulsion can also be used as a medium for electrochemical studies[11]. Recent work on bicontinuous microemulsions polymerization has been further extended to the preparation of porous polymeric materials which have potential applications in separation technology[12–24].

* To whom correspondence should be addressed

The microstructure of polymeric materials can be controlled by varying one or more of the component(s) of the precursor bicontinuous microemulsions. In our previous study[24], we found that the microstructure of the polymeric materials depends on the alkyl chain lengths of the cationic surfactants. The longer the alkyl chain length of the surfactants, the larger are the aggregates and pore sizes of the polymeric materials obtained. In this work, we extended our previous work[24] by investigating the effect of mixing long with short alkyl chain length cationic surfactants on the morphology and microstructure of the final polymeric materials obtained.

EXPERIMENTAL

Materials

Methyl methacrylate (MMA) from BDH, and both 2-hydroxyethyl methacrylate (HEMA) and ethylene glycol dimethacrylate (EGDMA) from Merck were purified under reduced pressure to remove impurities and inhibitors before use. Dibenzyl ketone (DBK) of purity >98% was used as received. Hexyltrimethylammonium bromide (C_6TAB), dodecyltrimethylammonium bromide (C_{12}TAB) and cetyltrimethylammonium bromide (C_{16}TAB), all of purity >98%, were used as received. Ammonium persulfate (APS) and *N,N,N′,N′*-tetramethylethylene diamine (TMEDA) of purity greater than 98 and 99%, respectively, were used as received from Aldrich. Millipore water of conductivity *ca.* 1.0 $\mu S\,cm^{-1}$ was used.

Table 1 The effect of mixing C_{16}TAB and C_{12}TAB or C_6TAB on the appearance of the polymeric materials obtained

Microemulsion sample[a]	C_{16}TAB (wt%)	C_{12}TAB (wt%)	C_6TAB (wt%)	Appearance[b] BD	AD
C10	100	0	—	WY	Tl
C8D2	80	20	—	WY	Tl
C5D5	50	50	—	BY	C
C2D8	20	80	—	BY	C
D10	0	100	—	BY	C
C8H2	80	—	20	WY	Tl
C6H4	60	—	40	YW	Tl
C5H5	40	—	50	BY	C
C4H6	50	—	60	BY	C
C2H8	20	—	80	LB	C
H10	0	—	100	LB	C

[a] Weight ratio of MMA/HEMA was maintained at 1/4 and EGDMA was 4.0 wt% based on the total weight of MMA and HEMA added. Each sample consisted of 50% aqueous solution and 50 wt% MMA and HEMA. The aqueous solution contained 20 wt% cationic surfactant or combination of long and short alkyl chain length cationic surfactants

[b] BD, before drying; AD, after drying, YW, yellowish white; BY, bluish yellow; LB, light bluish; Tl, slightly translucent; C, clear

Preparation of microemulsions

The microemulsion samples, in principle, can be chosen from the transparent region of the phase diagram which have been determined in our previous study[24]. *Table 1* listed the microemulsion compositions used in this study. The weight ratio of MMA to HEMA was maintained at 1/4 while the amount of EGDMA was 4.0 wt% based on the total weight of MMA and HEMA. Each sample consisted of 50 wt% aqueous solution. The aqueous solution contained 20 wt% surfactant or combination of long and short alkyl chain length surfactants.

Polymerization

Each microemulsion sample was photoinitiated using DBK in a 5 ml-glass ampoule. DBK added was 0.3 wt% based on the total weight of each sample. After purging with nitrogen for *ca.* 10 min, each sample was sealed air-tight and then irradiated with u.v. light in a Rayonet Photochemical Reactor chamber (model RPR-100). The photopolymerization was carried out for a duration of 2 h at 35± 0.5°C.

Electron microscopy investigation

The morphology of the polymeric materials was examined using a Hitachi S-4100 Field Emission Scanning Electron Microscope (FESEM). For viewing the fractured surfaces of the polymerized samples, they were freeze-fractured in liquid nitrogen while for the surface morphology, they were used directly for examination. Prior to examination, all the samples were then attached to an SEM stub and vacuum dried before coating with a thin layer of gold using a Jeol ion-sputter JFC-1100 coater.

Swelling characteristics

The polymerized samples were cut into small pieces, and washed with a large quantity of methanol, and leached with hot water at 50°C until the conductivity of the effluent was the same as that of fresh millipore water. They were dried to a constant weight in a vacuum oven at room temperature. They were then swelled in water at 30°C until they reached equilibrium and their weight gains were recorded. Duplicate readings were taken for each sample. The equilibrium water content, EWC, expressed as a percentage is given by

$$\mathrm{EWC}(\%) = \frac{W - W_o}{W}$$

where W refers to the weight of the swollen polymer sample at an equilibrium swelling and W_o the weight of the dried polymer sample.

Permeability studies

For the permeability studies, polymer films were prepared from the precursor bicontinuous microemulsions (with compositions shown in *Table 1*) initiated by a very reactive redox initiating system (APS/TMEDA)[25] at 25°C. This was done by forming the microemulsion samples into thin films between two glass plates in an enclosed chamber filled with purified nitrogen gas. The redox initiator used was equimolar APS/TMEDA and the amount was always 13.1 mmol l^{-1} (0.3 wt%) based on the total weight of the aqueous phase for each microemulsion sample.

After 6 h of polymerization, the unconverted monomer and surfactant in the polymer films were leached out by washing them with millipore water at 50°C. The conductivity of the effluent water was measured using an Omega CM-155 conductivity meter with a cell constant of 1.0291 cm^{-1}. The washing was continued until the effluent had the same conductivity as the fresh millipore water.

The permeabilities of the polymer membranes were determined using a 0.01 M NaCl solution which had a conductivity of 5380 $\mu S\,cm^{-1}$. The measurements were conducted using a permeability cell as described elsewhere[26]. One of the compartments of the cell contained a certain volume of 0.01 M NaCl solution while the other was filled with the same volume of millipore water. The two liquids were separated by the porous membrane of 25 mm in diameter and a thickness of about 50–55 μm. The rise in the conductivity of the millipore water due to the transport of NaCl across the membrane was monitored by a conductivity meter as a function of time at 25°C. The liquids in both compartments of the cell were stirred by mechanical stirrers each at 500 rpm to minimize the concentration gradients within each compartment.

A quantitative representation of the permeability of the membranes was obtained by determining the mass transfer coefficient (K_m) for the transport of NaCl across the membrane. The expression for K_m for the transport of solute in dialysis cells assuming quasi-steady-state diffusion is well documented in the literature[27,28], i.e.

$$K_m = \frac{V_1 V_2}{A(t - t_o)(V_1 + V_2)} \ln \frac{(C_1 - C_2)_{to}}{(C_1 - C_2)_t}$$

where A is the membrane surface area permeable to the solute. C_1 and C_2 are the concentrations of NaCl in the compartments upstream and downstream of the membrane, V_1 and V_2 are the volumes of the compartments upstream and downstream of the membrane, t_o is the initial time, and t is the final time. The NaCl concentration in the downstream compartment at a given time t, $(C_2)_t$, was experimentally determined by measuring the conductivity of the solution, while $(C_1)_t$ in the upstream compartment was obtained by the mass balance.

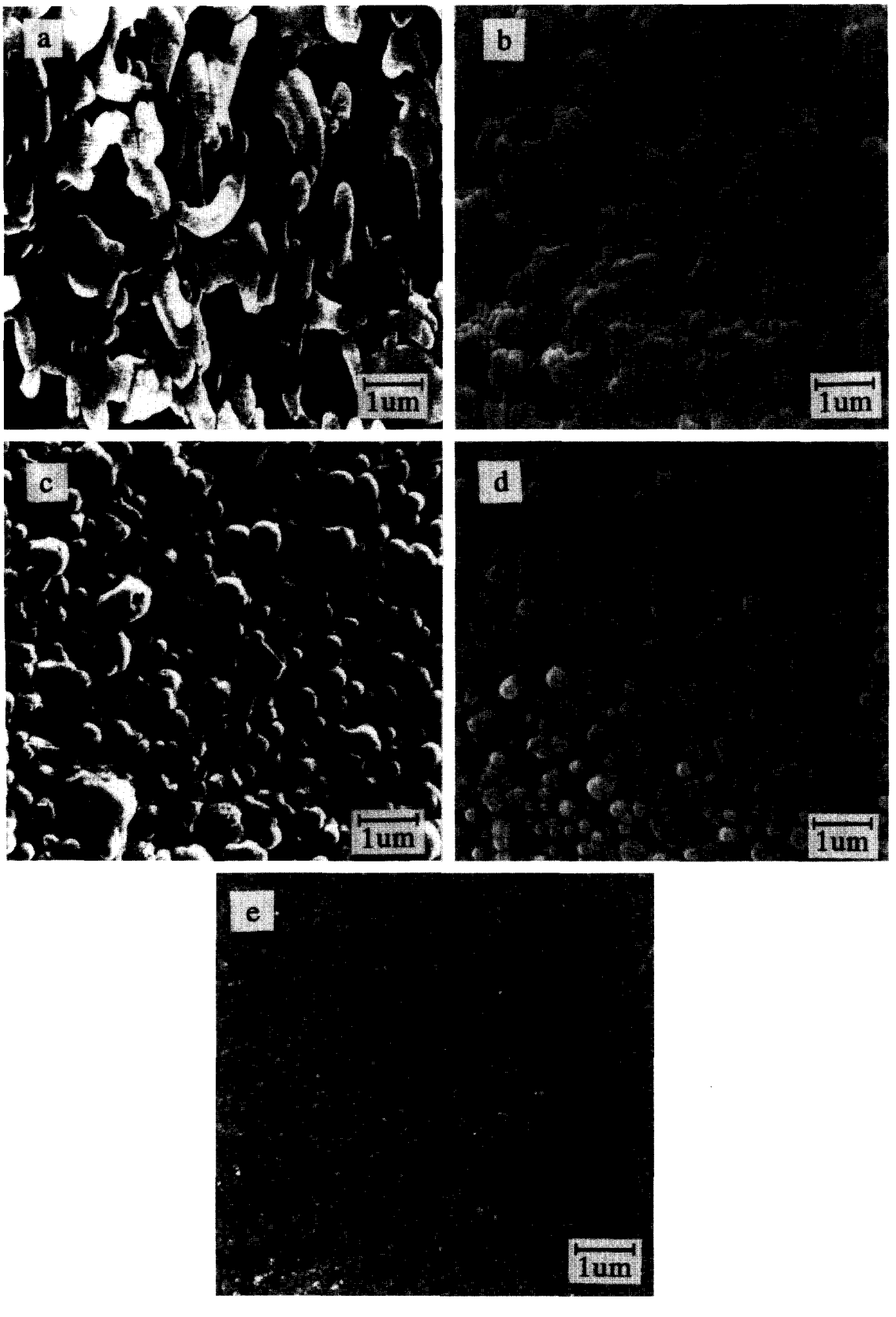

Figure 1 The surface morphology in contact with the glass wall for polymer samples: (a) C10; (b) C8D2; (c) C5D5; (d) C2D8; (e) D10

RESULTS

Polymerization

All the bicontinuous microemulsion compositions listed in *Table 1* were used for the polymerization study. The water content in each microemulsion sample was fixed at 40 wt%. This amount of water was employed because the microemulsions so formed exhibit the characteristics of bicontinuous structures as reported in the literature[15–18] and deduced from our previous studies[19,20].

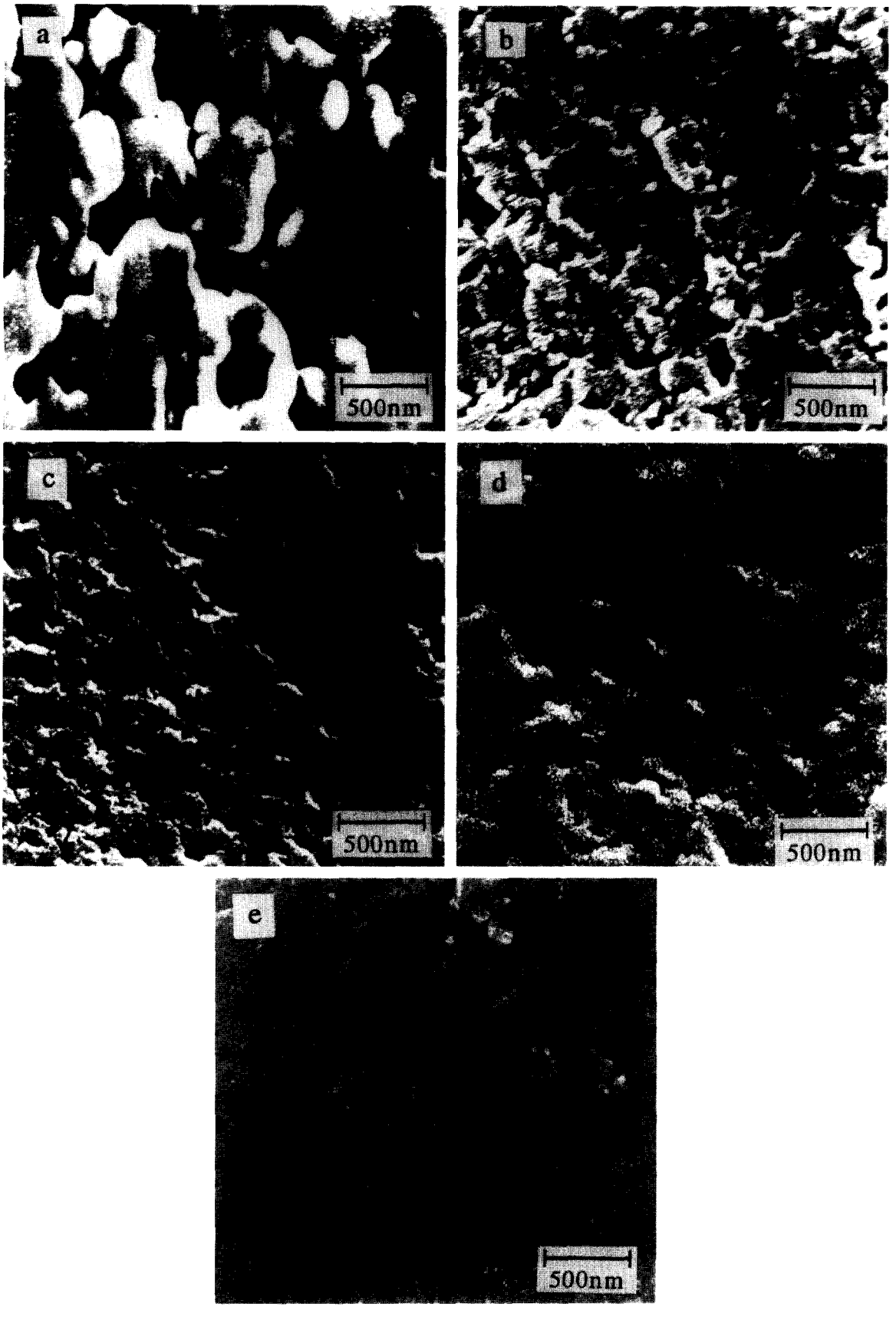

Figure 2 The morphology of the fractured surface for polymer samples: (a) C10; (b) C8D2; (c) C5D5; (d) C2D8; (e) D10

Upon the polymerization, the initial clear fluid microemulsion became more viscous until the formation of a transparent soft gel. On further polymerization, the clear soft gel turned into a solid whose appearance ranged from transparent, light bluish, bluish yellow or yellowish white depending on the composition of each microemulsion

sample. The opacity of the polymeric materials diminished on increasing the weight ratio of C_6TAB to $C_{16}TAB$ or $C_{12}TAB$ to $C_{16}TAB$ as shown in *Table 1*. Upon drying in an oven at 100°C for *ca.* 30 min, polymeric materials that were most opaque became slightly translucent, whereas those of low opacity changed to optically clear. However, when water was allowed to reabsorb into these dried polymeric materials, they resumed their original appearance.

Characterization of polymeric materials

The effect of mixing $C_{12}TAB$ with $C_{16}TAB$ in precursor bicontinuous microemulsions (with compositions shown in *Table 1*) on the microstructure of the polymeric materials is presented in *Figures 1* and *2*. *Figure 1(a–e)* shows the morphology of the surface in contact with the glass wall for polymer samples C10, C8D2, C5D5, C2D8 and D10, respectively, whereas *Figure 2(a–e)* shows their respective fractured surfaces. Some deformation of the microstructures arising from the fracturing process can also be seen from the micrographs for the fractured surfaces of the polymeric materials. Since the morphology of the polymer surfaces facing the glass wall or facing the nitrogen atmosphere were unaffected by the fracturing process, thus they present the more original microstructure of the polymer surfaces. As a result, the explanation as presented here on the transformation of microstructures of the polymeric materials containing different weight ratio of short and long alkyl chain length cationic surfactants was based on the polymer surfaces facing the glass wall. For polymer sample C10 which contained 100% $C_{16}TAB$, elongated, worm-like structures interconnected together with some oval-shaped and globular structures were observed in the micrograph as shown in *Figure 1a*. These worm-like structures were *ca.* 1–2 μm in length and *ca.* 0.2–0.5 μm in diameter. The corresponding fractured surface as depicted in *Figure 2a* shows the existence of porous structures. These pores were observed to be irregular in structure and were *ca.* 0.5–1.0 μm in length and *ca.* 0.05–0.2 μm in width. On increasing the weight ratio of $C_{12}TAB/C_{16}TAB$ to 1/4 (sample C8D2), oblate structures of dimension

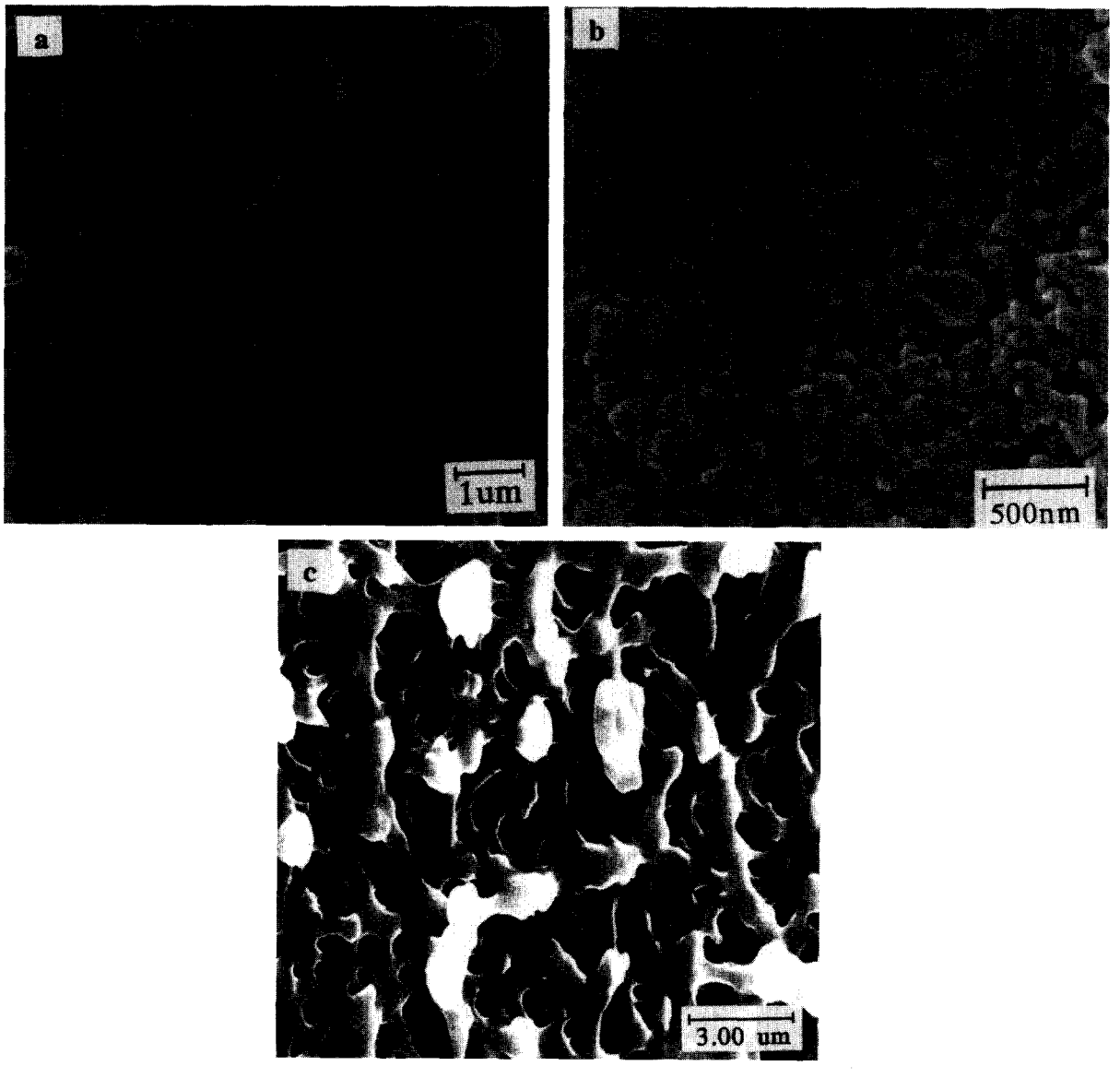

Figure 3 The morphology of polymer sample C6H4: (a) the surface in contact with the glass wall; (b) the fractured surface; (c) the surface facing nitrogen atmosphere

ca. 0.4–0.6 μm in length and *ca.* 0.2–0.3 μm in diameter (*Figure 1b*) were obtained with pore sizes in the range of *ca.* 50–300 nm (*Figure 2b*). When equal amounts of C_{16}TAB and C_{12}TAB were incorporated into the system (sample C5D5), globular structures of *ca.* 0.1–0.5 μm in diameter and pore sizes of *ca.* 50–100 nm were seen: see *Figures 1c* and *2c*, respectively. On further increase in the weight ratio of C_{12}TAB to C_{16}TAB, the globular microstructures for sample C2D8 (*Figure 1d*) became even smaller, but larger in size than those of sample D10 (*Figure 1e*) which used only C_{12}TAB. The pore sizes for both samples C2D8 and D10 were mainly within the range of *ca.* 20–100 nm as shown in *Figure 2(d* and *e)*.

When the much shorter chain length C_6TAB was used to replace C_{12}TAB, the effect on the microstructures of the polymeric materials was more pronounced, as illustrated in *Figures 3* and *4*. For instance, the morphology of the polymer surface facing the glass wall for polymer sample C8H2 (which contains 20% C_6TAB) was aggregated globular structures of size in the range 0.2–1.0 μm as shown in *Figure 3a*. The result was different from oblate structures observed for polymer sample C8D2 containing 20 wt% C_{12}TAB. The corresponding fracture surface shows pore size of *ca.* 50–200 nm as depicted in *Figure 3b*, while its surface facing the nitrogen atmosphere shows pores nearly round in shape, of dimension 0.5–2.0 μm can be clearly seen from *Figure 3c*. On further increasing the weight ratio of C_6TAB to C_{16}TAB as for samples C6H4, C5H5, C4H6, C2H8 and H10, the microstructures remained in globular form but their globular sizes became progressively smaller. However, only at particular weight ratios of C_6TAB to C_{16}TAB, for example, polymer sample C6H4, well defined pores or voids similar to random or sponge-like bicontinuous structures as reported in the literature[2,5] were observed as depicted in *Figure 4 (a–c)*. The pores were *ca.* 0.1–1.0 μm in length and *ca.* 50–200 nm in width. The solid polymer phase consisted of spherical globules aggregates. The larger globules (200 nm) are actually

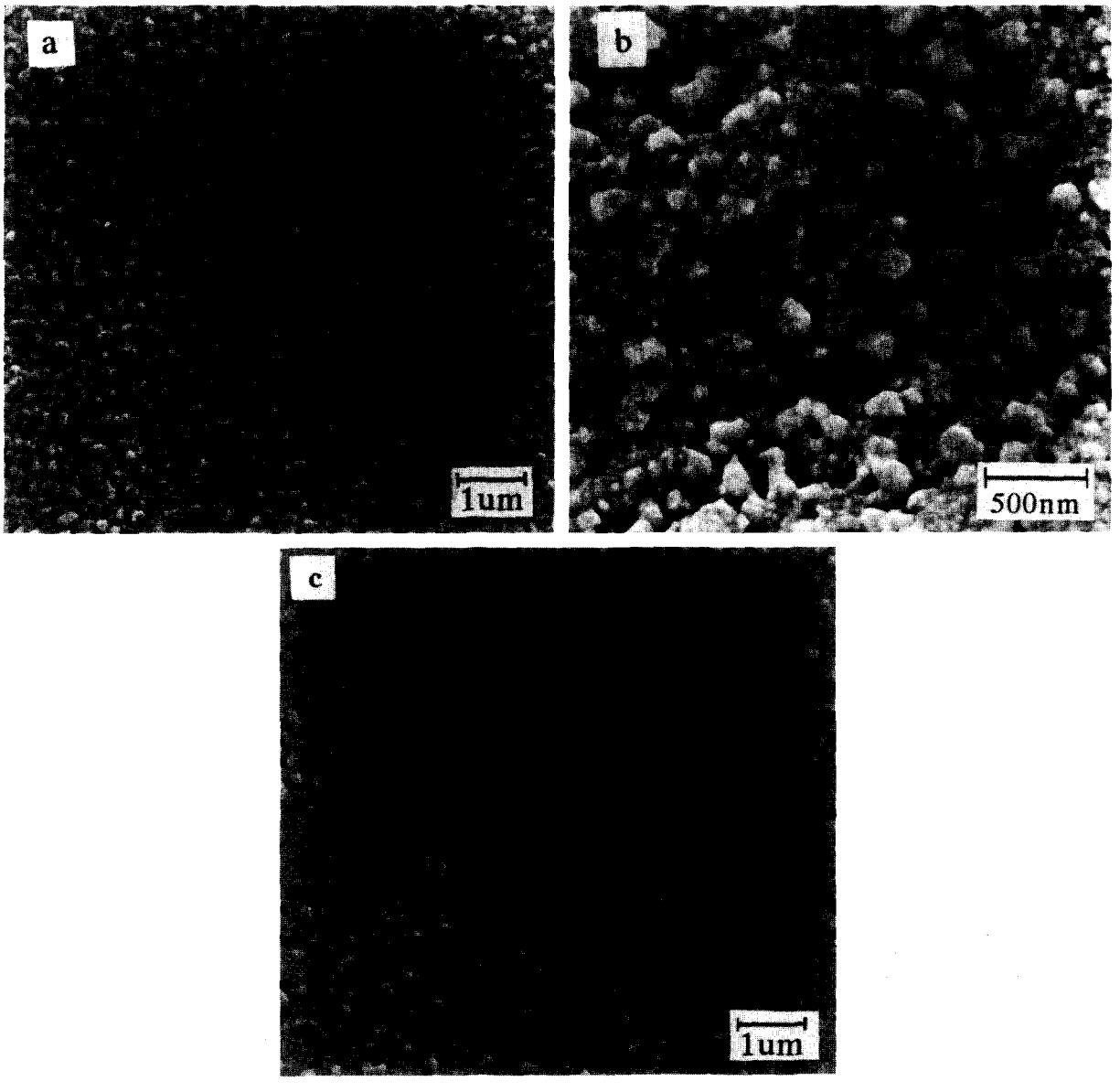

Figure 4 The morphology of polymer sample C6H4: (a) the surface in contact with the glass wall; (b) the fractured surface; (c) the surface facing the nitrogen atmosphere

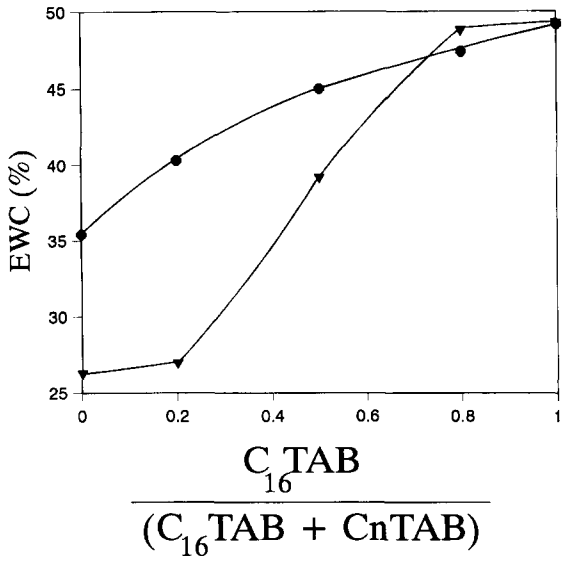

Figure 5 The effect of mixing C_6TAB or $C_{12}TAB$ with $C_{16}TAB$ on the equilibrium water content (EWC) of the polymeric materials (—▼—: $n = 6$; —●—: $n = 12$)

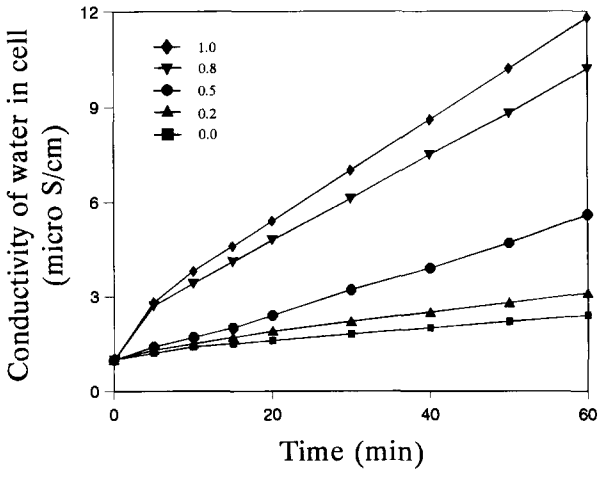

Figure 6 The permeability of the polymer membranes as measured by the rise in conductivity using a permeability cell. The symbols shown in the inset of the figure indicate the values of the weight ratio of $C_{16}TAB/(C_{16}TAB + C_6TAB)$

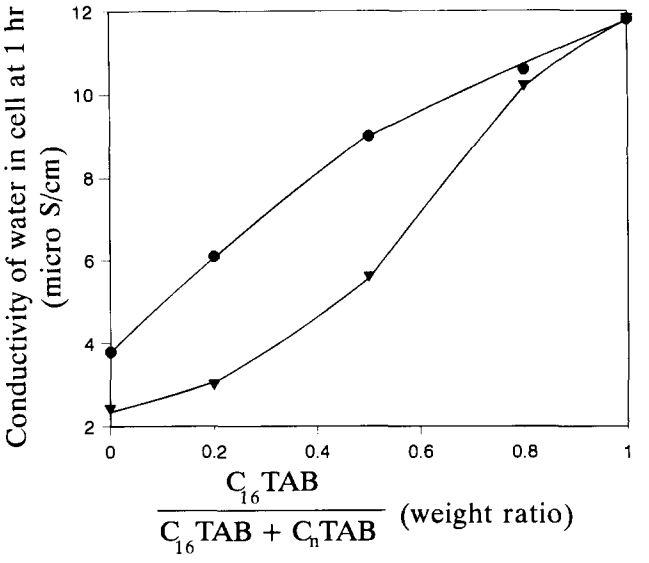

Figure 7 The effect of the weight ratio of $C_{16}TAB/(C_{16}TAB+C_nTAB)$ in polymer membranes on the permeability of the membranes measured in conductivity as for *Figure 5* (—▼—: $n = 6$; —●—: $n = 12$)

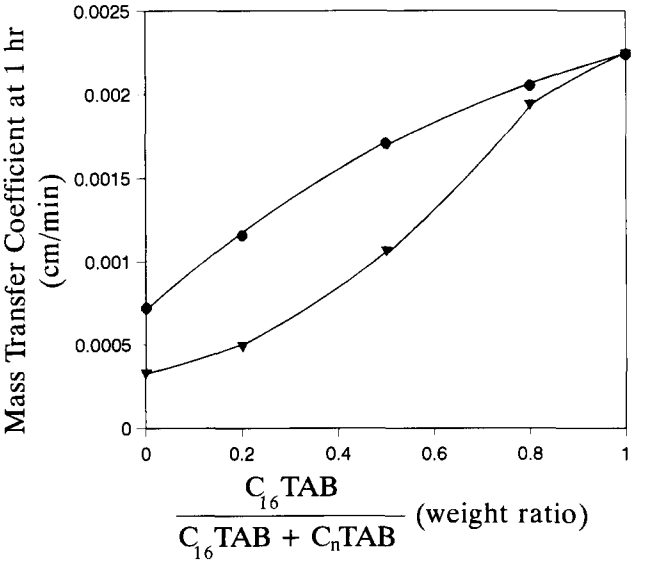

Figure 8 Mass transfer coefficient (K) for the transport of NaCl across membranes as a function of the weight ratio of $C_{16}TAB/(C_{16}TAB+C_nTAB)$ in polymer membranes (—▼—: $n = 6$; —●—: $n = 12$)

comprised of smaller globules which are coagulated with each other. Similar pore structures were also observed for polymer sample C4H6 (micrograph not presented here). It appeared that well-defined random bicontinuous pore structures were only observed at a suitable weight ratio of long and short alkyl chain length of *n*-alkyltrimethylammonium bromide (C_nTAB).

The effect of mixing C_6TAB or $C_{12}TAB$ with $C_{16}TAB$ on the EWC is presented in *Figure 5*. With the addition of a shorter chain length C_6TAB or $C_{12}TAB$ to $C_{16}TAB$, the EWC of the system decreased substantially, especially for the one with the shortest chain length.

The different permeabilities of the polymer membranes containing different weight ratios of C_6TAB with $C_{16}TAB$, as measured by the rise in conductivity using a permeability cell, are shown in *Figure 6*. It is clearly shown that higher conductivities were obtained for those polymeric membranes with higher weight ratio of $C_{16}TAB$ to C_6TAB. Similar results were also obtained from mixing $C_{12}TAB$ with $C_{16}TAB$. The permeabilities (measured after 1 h) of the membranes formed from microemulsions containing different weight ratio of $C_{16}TAB/(C_{16}TAB + C_6TAB)$ or $C_{16}TAB/(C_{16}TAB+C_{12}TAB)$ are summarized in *Figure 7*. The mass transfer coefficient (K_m) for the transport of NaCl across the membrane can be regarded as a quantitative measure of the permeability of the membranes. Thus, the effect of $C_{16}TAB/(C_{16}TAB + C_6TAB)$ or $C_{16}TAB/(C_{16}TAB+C_{12}TAB)$ weight ratio on K_m as plotted in *Figure 8* is similar to that of *Figure 7*.

DISCUSSION

The opacity of the polymeric materials diminished on increasing the weight ratio of $C_{12}TAB$ to $C_{16}TAB$. This is attributed to the decrease in size of both the aggregates

and pores as evinced from the electron micrographs. The pores or voids of the polymeric materials were water-filled spaces between the incompletely coalesced aggregates. It is envisaged that the aggregates were formed through the coagulation between polymer particles during the course of polymerization. As explained in our earlier study[24], the coagulation between the polymer particles is believed to take place through the strong attractive hydrophobic interactions. The formation of these incompletely coalesced aggregates is believed to be due to the presence of repulsive forces between the surfactant molecules adsorbed on the surfaces of each polymer particle. From the packing point of view, bigger pores will be formed between larger aggregates, while smaller pores will be generated from the coagulation of smaller aggregates. The addition of C_6TAB or C_{12}TAB to the system containing C_{16}TAB was found to reduce the sizes of aggregates and thus the pore sizes of the porous materials.

An increase in EWC on increasing the ratio of long to short alkyl chain length cationic surfactants indicated the increase in pore sizes of the polymeric materials. This was further substantiated by the permeability studies which support that the pore sizes of the polymeric materials increase with the increase in the ratio of long to short alkyl chain length cationic surfactants. All the FESEM observations, swelling characteristics and permeability studies of the polymeric materials showed an increase in pore sizes on increasing the ratio of long to short alkyl chain length cationic surfactants.

The micrographs also provide evidence of the polymerization-induced structural modifications from the initial isotropic bicontinuous phase to the final elongated, oblate and spherical aggregates depending on the mixing ratio of a short and long alkyl chain length of C_nTAB. Our previous studies[21] also showed that the polymerization of MMA and HEMA in bicontinuous microemulsion stabilized by C_{12}TAB would lead to the formation of spherical or globular structure aggregates. But we have also successfully prepared bicontinuous microstructures of transparent polymers recently by using polymerizable surfactants[19,22]. A mention should be included here regarding the polymerization of monomer in a lyotropic bicontinuous cubic phase with preservation of its precursor microstructures[30]. This was attributed to the extremely viscous nature of the phase which minimized the rearrangement of the microstructure during polymerization.

Several factors are responsible for microstructural modification during polymerization. It is known that the exothermic character of vinyl polymerizations undergoing a gel transformation can easily lead to large temperature excursions[31,32]. Thermal disruption during polymerization is inevitable for this kind of vinyl polymerization undergoing gel transformation during polymerization. Since the oil–water interfaces of bicontinuous microemulsions are flexible and fluctuating[33], they can easily undergo deformations. The second important factor involved in the microstructural change arises from the co-monomer HEMA. A notable extension of the microemulsion region on addition of HEMA into the system was observed in our previous study[24], indicating that HEMA possesses the characteristics of a cosurfactant. This means that HEMA is partially located between the surfactant molecules resulting in a flexible interfacial film, which favours the formation of bicontinuous microemulsion. As soon as polymerization starts the depletion of HEMA from the interfacial layers will cause an increase in the rigidity of the interfacial film. This is because the tail of the surfactant molecules become more closely packed with each other and the interfacial film is harder to bend[34] in the absence of HEMA.

On increasing the weight ratio of C_{12}TAB to C_{16}TAB, the bending rigidity constant (K) of the surfactant monolayer decreases. This can be understood from the considerations of interfacial film packing constraints. According to Bellocq and Jousset-Dubien[35], the bending rigidity constant (K) is related to the interfacial thickness (L) and the area per polar head (A):

$$K \propto \frac{L^n}{A^p}$$

where n and p are constants ($n \sim 2$–$3, p \sim 5$). The equation indicates that the thicker the interfacial film, the higher the K value. The presence of a shorter chain length surfactant at the interface would naturally lower the thickness of the interfacial film. This is because beyond the region packed by the short chain length surfactant molecules, the tails of the longer chain length surfactants are now essentially dangling free. The resulting effect of the decreased thickness of the mixed film in the presence of shorter chain length surfactant molecules is an increase in the flexibility of the monolayer film and so a smaller K value associated with it. This may explain why the microstructure changed progressively from elongated worm-like to oblate and to spherical structures on increasing the weight ratio of C_{12}TAB to C_{16}TAB.

When an even shorter chain surfactant, C_6TAB, was used to replace C_{12}TAB, the morphology of the polymeric materials obtained shows a sponge-like porous structure resembling that of the random bicontinuous structure of bicontinuous microemulsions. It should be noted here that the short alkyl chain length C_6TAB is not a micelle-forming surfactant due to its short hydrophobic moiety and high solubility in water. As a result, C_6TAB can only act as a cosurfactant. A suitable weight ratio of short and long alkyl chain length of cationic surfactants appears to be required to preserve the flexibility and degree of bending of the oil–water interfaces of the precursor systems once polymerization starts. In the absence of short chain length C_6TAB, the initial flexible mixed surfactant interfacial film will become more rigid when HEMA is moved away from the interfacial layers upon polymerization. This results in an increase of the thickness of the interfacial film which makes it difficult to bend thus unfavourable for forming spherical globules. However, when C_6TAB is mixed with C_{16}TAB, the change in the flexibility of the interfacial film may not be so drastic when HEMA is consumed from the surfactant monolayers after polymerization as compared to that in the presence of C_{12}TAB. This is because the shorter chain length C_6TAB will maintain a thinner interfacial film than is possible with C_{12}TAB.

The larger polymer aggregates observed at a higher ratio of C_{16}TAB to C_{12}TAB or C_6TAB are probably due to the fact that a surfactant with a longer alkyl chain length is more effectively anchored to the polymer surfaces. This is because a longer alkyl chain length surfactant will give rise to a greater hydrophobic

interaction with polymer compared to that of a shorter alkyl chain length surfactant. Thus the rate of mutual coagulation between the polymer particles is reduced. Hence, these polymer particles can grow to larger sizes before the coagulation occurs. On the other hand, a shorter alkyl chain length surfactant is less effective in preventing the coagulation with the neighbouring particles before the polymer particles can grow to larger sizes. Thus smaller particles are observed for the system using a higher ratio of a shorter alkyl chain length surfactant.

CONCLUSIONS

This study indicates the feasibility of preparing porous polymeric materials of controlled microstructures by simply polymerizing monomer(s)-containing bicontinuous microemulsions using mixtures of long and short alkyl chain length cationic surfactants. The morphology and microstructure of the polymeric materials formed in microemulsions is strongly dependent on the ratio of long and short alkyl chain length cationic *n*-alkyltrimethylammonium bromide surfactants. Mixing of short and long chain surfactants leads to a change in interfacial film packing constraints and thus to its bending rigidity constant. A suitable ratio of long and short alkyl chain length cationic surfactants can lead to the formation of well defined random or sponge-like bicontinuous structures. The control of microstructure through mixing of short and long alkyl chain length surfactants is more effective than using different alkyl chain length surfactants.

ACKNOWLEDGEMENT

The authors thank the National University of Singapore for providing financial support under grant no. RP 890638.

REFERENCES

1 Scriven, L. E. *Nature* 1974, **263,** 123
2 Jahn, W. and Strey, R. *J. Phys. Chem.* 1988, **92,** 2294
3 Bellocq, A. M., Bias, J., Clin, B., Lalanne, P. and Lemanceau, B. *J. Colloid Interface Sci.* 1979, **70,** 524
4 Lindman, B., Stilbs, P. and Moseley, M. E. *J. Colloid Interface Sci.* 1981, **83,** 569
5 Friberg, S. E., Lapczynska, I. and Gillberg, G. *J. Colloid Interface Sci.* 1976, **56,** 19
6 Talmon, Y. and Prager, S. *J. Chem. Phys.* 1978, **69,** 2984
7 De Gennes, P. G. and Taupin, C. *J. Phys. Chem.* 1982, **86,** 2294
8 Auvray, L., Cotton, J. P., Ober, R. and Taupin, C. *J. Phys.* 1984, **45,** 913
9 Candau, F., Zekhnini, Z. and Durand, J. P. *J. Colloid Interface Sci.* 1986, **114,** 398
10 Holtzscherer, C. and Candau, F. *J. Colloid Interface Sci.* 1988, **125,** 97
11 Iwunze, M. O., Sucheta, A. and Rusling, J. F. *Anal. Chem.* 1990, **62,** 644
12 Haque, E. and Qutubuddin, S. *J. Polym. Sci, Part C: Polym. Lett.* 1988, **26,** 429
13 Qutubuddin, S., Haque, E., Benton, S., J. and Fendler, E. J., in 'Polymer Association Structures: Microemulsions and Liquid Crystals' (Ed. M. A. El-Nokaly), ACS Symp. Series 384, Washington DC, 1989, p. 64
14 Sasthav, M. and Cheung, H. M. *Langmuir* 1991, **7,** 1378
15 Palani, W. R., Sasthav, M. and Cheung, H. M. *Langmuir* 1991, **7,** 2586
16 Palani, W. R., Sasthav, M. and Cheung, H. M. *Langmuir* 1992, **8,** 1931
17 Palani, W. R., Sasthav, M. and Cheung, H. M. *Polymer* 1993, **34,** 3305
18 Palani, W. R., Sasthav, M. and Cheung, H. M. *J. Appl. Polym. Sci.* 1993, **47,** 499
19 Gan, L. M., Chieng, T. H., Chew, C. H. and Ng, S. C. *Langmuir* 1994, **10,** 4022
20 Chieng, T. H., Gan, L. M., Chew, C. H. and Ng, S. C. *Polymer* 1995, **36,** 1941
21 Chieng, T. H., Gan, L. M., Chew, C. H., Lee, L., Ng, S. C., Pey, K. L. and Grant, D. *Langmuir* 1995, **11,** 3321
22 Li, T. D., Gan, L. M., Chew, C. H. and Teo, W. K. *J. Macromol. Sci., Pure Appl. Chem.* 1995, **A32,** 969
23 Burhan, J. H., He, M. and Cussler, E. L. *AIChE J.* 1995, **41,** 907
24 Chieng, T. H., Gan, L. M., Chew, C. H., Lee, L., Ng, S. C., Pey, K. L. and Grant, D. *Polymer* (in press)
25 Guo, X. Q., Qiu, K. Y. and Feng, X. D. *Makromol. Chem.* 1990, **191,** 577
26 Sakai, K. *J. Membrane Sci.* 1994, **96,** 91
27 Geankoplis, C. J. in 'Transport Processes and Unit Operations', Allyn and Bacon, Boston, 1983, Chap. 6, p. 390
28 Bidstrup, D. E. and Geankoplis, C. J. *J. Chem. Eng. Data* 1963, **8,** 170
29 Tsutui, T. and Tanaka, T., *J. Polym. Sci., Polym. Lett. Ed.* 1977, **15,** 475
30 Anderson, D. M., and Strom, P. in 'Polymer Association Structures: Microemulsions and Liquid Crystals' (Ed. M. A. El-Nokaly), ACS Symp. Series 384, Washington DC, 1989, p. 204
31 Armitage, P. D., Hill, S., Johnson, A. F., Mykytink, J. and Turner, J. M. C. *Polymer* 1988, **29,** 2221
32 Driscoll, K. F. O. and Huang, J. *Eur. Polym. J.* 1990, **26,** 643
33 di Meglio, J. M., Dvolaitzky, M., and Taupin, C. *J. Phys. Chem.* 1985, **89,** 871
34 Szleifer, I., Kramer, D., Ben-Shaul, A., Gelbarat, W. M. and Safran, S. A. *J. Chem. Phys.* 1990, **92,** 6800
35 Bellocq, A. M. and Joussot-Dubien, M. *J. Disp. Sci. Technol.* 1992, **13,** 169